## Originally published as:

**Kornhuber, K., Petoukhov, V., Petri, S., Rahmstorf, S., Coumou, D. (2017):** Evidence for wave resonance as a key mechanism for generating high-amplitude quasi-stationary waves in boreal summer. - Climate Dynamics, 49, 5-6, 1961-1979

**DOI:** 10.1007/s00382-016-3399-6

# Evidence for wave resonance as a key mechanism for generating high-amplitude quasi-stationary waves in boreal summer

***K. Kornhuber[1, 2*], V. Petoukhov[1], S. Petri[1], S. Rahmstorf[1, 2], D. Coumou[1]***

*[1]Potsdam Institute for Climate Impact Research – Earth System Analysis, Telegrafenberg A 31, 14473 Potsdam, Germany*

*[2]Universität Potsdam, Am Neuen Palais 10, 14469, Potsdam, Germany*

**Corresponding author (contact information: kai.kornhuber@pik-potsdam.de)*

## Abstract

Several recent northern hemisphere summer extremes have been linked to persistent high-amplitude wave patterns (e.g. heat waves in Europe 2003, Russia 2010 and in the US 2011, Floods in Pakistan 2010 and Europe 2013). Recently quasi-resonant amplification (QRA) was proposed as a mechanism that, when certain dynamical conditions are fulfilled, can lead to such high-amplitude wave events. Based on these resonance conditions a detection scheme to scan reanalysis data for QRA events in boreal summer months was implemented. With this objective detection scheme we analyzed the occurrence and duration of QRA events and the associated atmospheric flow patterns in 1979 – 2015 reanalysis data. We detect a total number of 143 events for wave 6, 7 and 8 and find that during roughly one third of all high amplitude events QRA conditions were met for respective waves. Our analysis reveals a significant shift for quasi-stationary waves 6 and 7 towards high amplitudes during QRA events, lagging first QRA-detection by typically one week. The results provide further evidence for the validity of the QRA hypothesis and its important role in generating high amplitude waves in boreal summer.

## I. Introduction

Observations show a rise in the frequency and severity of heat extremes and heavy rainfall events in the NH mid-latitudes (Coumou & Robinson 2013; Min et al. 2011; Westra et al. 2013; IPCC 2012; Hansen et al. 2012). Those events often imply massive humanitarian and economic impacts (Coumou & Rahmstorf 2012). As anticipated by basic thermodynamics, the frequency of extreme temperatures and heavy rainfall events is expected to increase in a warming climate (Rahmstorf & Coumou 2011; Christidis et al. 2014; Min et al. 2011). As the mean temperature shifts towards higher values, record-breaking or threshold exceeding temperatures will become more common (Coumou & Robinson 2013; Coumou et al. 2013). Furthermore, warmer air can hold more water vapor, which in turn leads to an increase of heavy rainfall events on a global scale (Westra et al. 2013; Lehmann et al. 2015; Fischer & Knutti 2015).

Still, some of the recent weather extremes go beyond what would be expected by a simple shift of the distribution. Luterbacher et al. (2004) estimated a return period for an extreme event as the 2003 European heatwave of about 100 years. Yet, this event has already been exceeded in the same decade by the 2010 Moscow heatwave (Dole et al. 2011; Christidis et al. 2014) which was recently quantified as the most-intense heat wave in a global analysis (Russo et al. 2014). During the extreme events mentioned above, the mid-latitude circulation was characterized by anomalously persistent meandering patterns of the circumglobal jet stream. Hemisphere-wide, high-amplitude waves remained in the same longitudinal position for several weeks and thereby caused continental scale extreme weather conditions (Petoukhov et al. 2013; Coumou et al. 2014; Ogi et al. 2005; Tachibana et al. 2010; Lau & Kim 2012; Black et al. 2004).

These cases of anomalous summer weather suggest that in addition to thermo-dynamical effects, dynamical processes such as changes in the characteristics of the extratropical jet streams and atmospheric waves play a role for the observed increase of frequency and severity of recent Northern hemisphere Summer weather extremes (Tachibana et al. 2010; Schubert et al. 2011; Petoukhov et al. 2013; Coumou et al. 2014; Ogi et al. 2005; Palmer 2013; Stadtherr et al. 2016). Indications of dynamical changes of the NH summer circulation have been reported by several studies (Overland et al. 2012). Coumou et al. (2015) report a weakening of several key characteristics like zonal mean zonal wind, kinetic energy of transient synoptic eddies and the amplitude of fast moving Rossby waves over 1979 - 2014. Using self-organizing maps cluster analyses, Horton et al. (2015) show that in summer the frequency of anticyclonic circulation over Europe, western Asia and eastern North America has increased and also that they persist longer. However, they analyze 500mb geopotential heights and it remains questionable whether the reported changes are truly dynamical effects or due to thermal expansion of the lower troposphere or a combination of both. Still, such dynamical changes might have contributed to prolonged heat extremes in these regions, but a physical mechanism for the prolonged duration of these regional anticyclonic flow patterns is not provided.

Quasi-resonant wave amplification (QRA) has been suggested as a mechanism that could lead to simultaneous blocking events within the mid-latitudes by trapping and amplifying slow moving waves (Petoukhov et al. 2013). This internal atmosphere-dynamical mechanism invokes the resonance between different wave types leading to their amplification.

In general, the large-scale azonal mid-latitudinal atmospheric circulation is characterized by two kinds of waves:

i) Synoptic-scale Rossby waves.

These waves wave numbers 6 and higher, relatively large phase speeds (eastward propagation of the order of 6 -12 m/s) and only a small quasi-stationary component (Schneider et al. 2014). Once originated, they don't require any forcing to be maintained and are thus referred to as *free waves*. Mathematically these waves can be described by the azonal stream-function equation with zero right hand side (i.e. no forcing). The second component is composed by

ii) *forced waves*.

These waves are the outcome of quasi-stationary diabatic or orographic forcings. As the large-scale forcing patterns change on substantially longer timescales of several weeks, these waves can be considered quasi-stationary with typical wave numbers smaller than 6. Normally, the forced quasi-stationary component of wave numbers 6-10 is weak and their energy is effectively dispersed towards the poles and equator. However, during a number of recent summers featuring severe weather events (including the European heatwave of 2010 and the Moscow heatwave of 2010), zonally elongated trains of high-amplitude quasi-stationary waves of wave numbers 6-8 were observed (Petoukhov et al. 2013). If the latitudinal distribution of the zonal mean zonal wind distribution in the mid-latitudes exhibits specific characteristics (detailed description provided in Sec.II) the synoptic scale quasi-stationary free waves can almost completely be trapped within the mid-latitudes. This prevents the rapid dissipation and meridional dispersion of their energy, thus leading to their confinement in the mid-latitudes.

This occurs when two mid-latitude reflection (or turning) points emerge for these waves at different latitudes. Such constellation of turning points is referred to as a waveguide (Hoskins & Karoly 1981; Ambrizzi et al. 1995). If additionally the trapped free waves have similar length-scales as the quasi-stationary forcings a pronounced magnification of the slow moving forced waves can occur due to resonance. This is the essence of QRA. This can lead to hemispheric-wide persistent blocking patterns in the mid-latitudes with unusual high amplitudes of zonal wave numbers 6, 7 or 8, as observed during several recent extreme weather events (Petoukhov et al. 2013; Coumou et al. 2014).

The QRA hypothesis builds upon the classical work by Hoskins & Karoly (1981) but, in its current version takes a zonal-mean approach with respect to waveguides. We do so in order to explain recent anomalous circulation patterns which were circumglobal and starkly zonally oriented. Limitations of this approach are further discussed in the discussion (Sec IV.).

As the NH circulation exhibits strong seasonal differences (Archer & Caldeira 2008), with weaker zonal flow and wave phase speeds in summer, we focus on summer circulation, following previous studies analyzing QRA events (Petoukhov et al. 2013; Coumou et al. 2014) which used monthly-mean data and were limited to July and August only.

In this study, we present a novel detection scheme that, by employing the conditions derived by Petoukhov et al. (2013) can be used as a diagnostic tool to scan reanalysis datasets and climate model data for QRA events using 15-days running mean data.

After discussing the used data, relevant equations and QRA criteria (Sec. II.:  Methods), we apply the detection scheme to reanalysis data. We detect several QRA events, analyze their wave characteristics and test the statistical significance of the QRA-mechanism in causing high amplitude quasi-stationary waves (Sec. III.: Results). Furthermore, we analyze the most prolonged resonance events in detail and show that the majority were linked to documented extreme weather events. Moreover, we present statistical analyses linking resonance events to surface weather extremes in the mid-latitudes. We end with a discussion of the limitations of our approach and directions for future research

## II. Methods

### Data

We analyzed 15-days running mean data during summer months June, July and August (JJA) of 1979-2015 using the NCEP-NCAR reanalysis on a 2.5° x 2.5° grid (Kalnay et al. 1996). Temperature as well as zonal and meridional wind fields were analyzed at a pressure level of 300 mb. Orographic data was taken from Hastings & Dunbar (1999). Taking into account that the resulting forcing is much smoother than orography itself, it was coarsened to a 10° x 15° grid as in Charney & Eliassen (1949). Wave amplitudes were determined from reanalysis data by applying a zonal fast Fourier transformation (FFT) on the area-weighted meridional mean from 37.5 °N to 57.5° N for both daily meridional wind data and 15-days running mean meridional wind data. We calculated phase speed (eastward propagation) by applying a fourth-order accurate numerical approximation of the transient derivative of the waves' phase as in (Coumou et al. 2014).

**Quasi-resonant wave amplification**

In the following we give an overview of the theory behind the QRA hypothesis. For a detailed derivation of the equations we refer to Petoukhov et al. (2013). Quasi-resonant amplification of a forced wave with wave number $m$ requires a synoptic scale free wave with wave number $k \approx m$ to be trapped in a mid-latitude waveguide. Following the Wentzel-Kramers-Brillouin theory (WKB ) this waveguide has to meet certain characteristics in terms of width and position (Hoskins & Karoly 1981; Hoskins & Ambrizzi 1993; Dickinson 1970; Tung & Lindzen 1979). When a waveguide exists and the combined orographic and thermal forcing pattern is sufficiently large, then QRA can create a high-amplitude quasi-stationary wave with wave number $m$. Thus, the occurrence of QRA of wave number $m$ boils down to two necessities (s. Tab.1):

i. A waveguide for a wave number $k \approx m$ is present and

ii. the combined amplitude of thermal and orographic forcing (effective forcing) for wave number $m$ is of sufficient magnitude.

These two criteria specify whether resonance *conditions* are present. To test whether resonance has *occurred* we compare observed wave amplitudes with those given by an equation for wave amplitudes during QRA events as introduced by Petoukhov et al. (2013). Thus, for a single time step we test whether the *observed* wave amplitude is within a range given by the *calculated* amplitude expected for resonance (specified below). Only then an episode which fulfills conditions i. and ii. is considered a *QRA event*. This *Amplitude test* (AT) thus quantifies how often resonant amplitudes are actually observed when resonant conditions (i. and ii.) are fulfilled.

In the following each of the conditions i., ii. and the AT will be discussed in detail.

**i. Waveguide**

The formation of a waveguide depends solely on the square of the meridional wave number $l^2(U,\varphi)$. The quasi-linear barotropic vorticity equation on a sphere (Pedlosky 1979; Hoskins & Karoly 1981) for adiabiatic free waves at the equivalent barotropic level (EBL, i.e. about 300-500 mb) can be written as:

$$\left(\frac{\partial}{\partial t}+\frac{U}{a\cos\varphi}\frac{\partial}{\partial\lambda}\right)\Delta\psi+\left(2\Omega-\frac{1}{a\cos\varphi}U\right)\frac{\partial\psi}{\partial\lambda}=0, \qquad [1]$$

where $\lambda$ is the longitude, $\varphi$ the latitude, $t$ the time, $a$ is the earth radius, $\Omega$ the earth angular velocity and $U$ the zonal mean zonal wind. By applying WKB-theory and assuming quasistationary plane wave solutions (thus $\psi=\exp(i\frac{k}{a}x+ly-\ \omega t)$ with frequency $\omega\approx 0$) , $l^2$ can be expressed as:

$$l^2=\frac{2\Omega\cos^3\varphi}{aU}-\frac{\cos^2\varphi}{a^2U}\frac{d^2U}{d\varphi^2}+\frac{\sin\varphi\ \cos\varphi}{a^2U}\frac{dU}{d\varphi}+\frac{1}{a^2}-\left(\frac{k}{a}\right)^2, \qquad [2]$$

where $k$ is the zonal wave number (Petoukhov et al. 2013; Hoskins & Karoly 1981). Here, applying a 15-days running mean on $U$ is necessary to filter out fast moving transients.

The width of a waveguide is determined by the latitudinal positions of its two turning points (TP) at which $l^2$ changes sign (note that $l$ can both be real or imaginary). A mid-latitude waveguide is defined as such, when two TPs appear within the mid-latitudes with $l^2 > 0$ and $U > 0$ in between the TPs and also $U > 0$ in the vicinity of the TPs. In order for the WKB theory (and thus Eq. [2] to be valid), certain conditions apply to the shape and position of the waveguide:

The TPs are required to have a minimum distance of $w_k \approx 2°$ , so that the waveguide's width exceeds the characteristic scale of the relevant Airy function (Dingle 1973; Murdock 1987; Olver 1975; Hoskins & Karoly 1981). Additionally the WKB-approximation requires the change in the meridional wavelength ($dl/d\varphi$) over the latitudes to be small (smoothness of $l^2$) within the waveguide's interior (Petoukhov et al. 2013; Hoskins & Karoly 1981). To ensure this, the maximum value of $l^2$ in between the TPs is limited to a range defined by $l_{min}^2$ and $l_{max}^2$. Those values were determined as $l_{min}^2 = 10^{-13}$ m $^{-2}$ and $l_{max}^2 = 10^{-12}\mathrm{m}^{-2}$.

The maximum allowed value $l_{max}^2$ was implemented in order to exclude potential 'spikes' resulting from singularities when $U \approx 0$ (but $U > 0$). The minimum value $l_{min}^2$ was calculated by setting the maximum allowed meridional wave length to half of the earth's circumference (π radians).

If two waveguides are present for a certain wave number $k$, then their latitudinal distance has to be at least 5° in order to ensure full reflection within the waveguides and no propagation of the wave energy between the waveguides (Petoukhov et al. 2016). We calculated $l^2$ using Eq. [2] for $k$ values ranging from $5.5$ to $8.4$ with a step size of $0.1$ and applying a 15-days running mean to $U$. Latitude-positions of TPs, waveguide characteristics, and relative positions of several potential waveguides were determined for each day in the reanalysis period (1979 – 2015).

**ii. Effective Forcing**

In case a waveguide is present for a free synoptic wave with wave number $k$ (i.e. criterion $i$ is fulfilled), and under the assumption that the frictional force is acting mainly in the boundary layer (PBL), then Eq. [S14] from (Petoukhov et al. 2013) for the wave amplitude is valid:

$$A_m = \frac{A_{eff}}{\sqrt{[(k/a)^2 - (m/a)^2]^2 + (L/a^2 + R^2/L)^2 (m/a)^2}} \qquad [3]$$

Here, $m$ is the wave number of the forced wave, $R = \kappa R_0$ (with $R_0 = 0.135$) is the Rossby number for eddies dominantly contributing to the efficient atmospheric "eddy viscosity" (friction force in the PBL) and $L = \kappa L_0$ (with $L_0 = 6 \cdot 10^5$ m) is the characteristic Rossby radius of the above-mentioned eddies. The amplitude of the effective forcing $A_{eff}$ can be calculated by applying a zonal FFT on the area-weighted meridional average of the effective wave-forcing $F_{eff}$ :

$$A_{eff} = FFT\left(F_{eff}\right). \qquad [4]$$

With the effective wave-forcing $F_{eff}$ at $300$ mb calculated by employing Eq. [S1c] from (Petoukhov et al. 2013):

$$F_{eff} = \frac{2\Omega \cdot \sin(\varphi)\cos(\varphi)^2}{a \cdot T_c} \cdot \frac{\partial \hat{T}}{\partial \lambda} - \frac{2\Omega \cdot \sin(\varphi)\cos(\varphi)^2}{a \cdot H} \kappa \frac{\partial h_{or}}{\partial \lambda}, \qquad [5]$$

where $\lambda$ is longitude, $T_c = 200$ K is a constant reference temperature at the equivalent barotropic level (EBL), $\hat{T}$ is the 15-days running mean azonal temperature at 300 mb, $H = 12000$ m is the characteristic scale of the troposphere height, $\kappa$ = 0.4 is the characteristic value of the ratio of the zonally averaged zonal wind $U$ at 300 mb and the zonally averaged zonal wind at the mean orographic height and $h_{or}$ the coarse resolution orography.

In general both $k$ and $m$ are fractional (Hoskins & Karoly 1981). However, following the approach taken by Petoukhov et al. (2013) determining $A_{eff}$ via an FFT on $F_{eff}$ (Eq. [5]) results in integer values of $m$.

Apart from $k$ being close to $m$, for efficient amplification to take place, $A_{eff}$ has to be of sufficient magnitude. Therefore, $A_{eff}$ is determined for wave numbers $1-15$, and a threshold quantile $q_k$ is estimated. In our analysis we set this threshold to the median forcing, implying that the forcing for the trapped wave has to be among the strongest 60%.

An overview of the applied conditions is provided in Tab.1.

**Amplitude test**

As a test, we check whether the calculated wave amplitude (Eq. [4]) is close to those observed during periods when resonance conditions are fulfilled (i. + ii.). We calculate $A_m$ for $k = \mathrm{m} \pm 0.2$ giving an estimated range of wave amplitudes expected from resonance. When the observed wave amplitude falls within this range, the *Amplitude test* (AT) is passed. For $k = \mathrm{m} \pm 0.2$, Eq. [4] estimates typically rather high amplitudes $A_m$. Eq. [3] shows that the zonal wave number $k$ needs to be close to the zonal wave number $m$ of the forced wave. In that case the first term in the denominator is close to zero resulting in large values of $A_m$, i.e. strong amplification. Petoukhov et al. (2016) approximated the maximum difference $|k-m|$ to be between $0.25 - 0.30$ depending on wave number. This was determined by finding the maximum difference $|k-m|$ which leads to an amplitude $A_m$ of 1.5 $\sigma$ threshold above the 1979-2014 climatology, as calculated with Eq. [4] and with $A_{eff}$ set to the maximum observed value during 1979-2014. In our implementation a conservative approximation is applied, setting the maximum difference of $k - m = \pm 0.2$. This leads to a range of considered values of $k$ as follows: $k_6 = 5.8 - 6.2,\ k_7 = 6.8 - 7.2,\ k_8 = 7.8 - 8.2$ .

The AT thus tests whether the high amplitudes expected from resonance are actually observed. Due to the limitations of the approach as for example zonal mean field analyses or the use of linearized equations (see discussion) there can be cases a waveguide is detected but still the associated wave is not efficiently trapped.

We apply the AT to single clusters of consecutive days fulfilling the conditions i. and ii. only, and not to each individual day. The reason is that Eq.[3] provides a stationary solution for the eventual possible wave amplitude. However, it takes several days for resonance to amplify waves and thus the first days fulfilling i. and ii. don't necessarily show exceptional amplitudes. Also nonlinear processes such as Rossby wave breaking are not captured by Eq. [3].

QRA-clusters are defined as sequences of consecutive time steps meeting i. and ii. for at least one $k$. For a cluster of QRA days, the AT needs to be fulfilled for at least 25% of days which was found to give reasonable results.

**Mid-latitude Extreme index**

To quantify whether surface weather conditions are more extreme during QRA compared to normal conditions Coumou et al. (2014) defined a mid-latitude extreme (MEX) index:

$$MEX(x,t) = \left(\frac{1}{N}\sum_i^N \left(\frac{\Delta x_i(t)}{\sigma(x_i)}\right)^2 - \mu_{MEX}\right)/\sigma_{MEX}\ . \qquad [5\ ]$$

Here $\Delta x_i$ gives the anomaly of variable $x$ from its linear trend on a mid-latitudinal grid with $N$ grid points at time-step $t$, $\sigma(x_i)$ is the standard deviation of $x$ at grid point $i$. Normalization of the MEX index is done by subtraction of its time – averaged mean $\mu_{MEX}$ and division by its standard deviation $\sigma_{MEX}$. In our analysis the MEX index is applied on temperature data. Temperature anomalies were determined by subtracting the mean of the observed time period (1979 – 2015) of every grid point. To prevent that long-term trends influence the index we de-trend the data by a grid-point wise subtraction of the respective linear trend.

## III. Results

### Case studies: Extreme summers 2003 & 2010

The summer months of 2003 (European heatwave) and 2010 (Moscow heatwave) featured extraordinary continental scale heat extreme (Russo et al. 2014). Fig. 1 shows several zonally averaged dynamic variables in a Hovmöller diagram for the summer months June – August of 2003 and 2010. The 2003 heatwave lasted from July to August (Schär et al. 2004) with high surface temperatures across central and South Western Europe. Figure 1a plots the zonal mean zonal wind against time. Two peaks located at approximately 40°N and 70°N form in early July and persist until mid- August. In the following we will refer to such a constellation as a *double jet* pattern. Note that two peaks in the zonally averaged zonal wind do not necessarily represent two separate jets around the full hemisphere.  A pronounced meandering of the jet with reduced zonal wind between 40°N and 70°N could produce a similar zonal mean profile. Heat waves are reflected in the elevated zonally averaged surface temperatures in the mid-latitudes (Fig. 1b) at latitudes 55°N to 65°N. Fig. 1c shows the meridional wave number $l^2$ as calculated by Eq. [2] as a Hovmöller-plot. A waveguide forms at $\sim$40°N for wave 7 in mid-July (black solid line). As the forcing pattern is of sufficient magnitude, QRA is detected (i.e. i. + ii. +

AT fulfilled) for wave 7 from mid-July to mid-August (Fig. 1d). The detection of QRA precedes maximum amplitudes of the respective wave by about two weeks (Fig. 1e). As the waves require time to gain in amplitude, high values are observed for wave 7 in beginning of August. This coincides with the peak of the heatwave (Black et al. 2004), illustrated by the latitudinal broadening of high zonally averaged surface temperatures beginning in early August (Fig. 1b).

The evolution of the analyzed variables during the summer 2010 (Fig. 1f-j) are similar to those discussed above for 2003. This includes the formation of a double jet. In 2010 a double jet pattern formed (Fig. 1f) beginning of July prior to the formation of a waveguide (white solid line) for wave 6 (Fig. 1h) and QRA detection of wave 6 end of July / beginning of August (Fig. 1i). Wave 6 amplifies and reaches its peak amplitude approximately 2 weeks after QRA detection before weakening again in mid-August (Fig. 1j). Again a double peak in the zonally averaged zonal wind precedes wave amplification and the peak of the heatwave in mid-August (Fig. 1g). In the following section we will test the impact of QRA on causing high amplitude quasi-stationary waves statistically.

**Detected QRA events**

15-days running mean data of all summer days (JJA) of the period 1979-2015 were analyzed for QRA events. A QRA event is defined as a group of consecutive days fulfilling conditions i. and ii. and for which the AT was passed. Over 1979 - 2015 we detect a total of 143 QRA events totaling 1185 running mean days. With 82 events (495 time steps), most of them are wave 6 events followed by wave 7 (54 events, 503 time steps) and wave 8 (30 events, 81 time steps) (Tab. 2). Thus, compared to the other waves, wave 7 events have the longest duration per event with a mean duration of ten days. The forcing condition ii has the biggest impact on wave 6 reducing the number of single time steps by almost a third, while detected time steps for wave 7 and wave 8 are decreased only slightly. Here, the number of events is even increasing for those wave numbers. This is due to the 'splitting' of long events into two or more shorter ones in case the forcing is not sufficient over the full duration of a waveguide. 84% of all detected resonance condition events also meet the AT for wave 6, thus can be explained by QRA. This value is smaller for wave 7 (47%) and wave 8 (38%).

As illustrated in the histogram of the event duration for each condition, most of the detected events are short events (1 day – 8 days) (Fig. 2). When focusing on long duration events (> 9 days) the ratio of events meeting the AT is increasing to 90% (wave 6), 63 % (wave 7) and 50% (wave 8) (Tab.3). A total of 47 long duration events (> 9 days) were detected containing 760 single time steps, which accounts for about 20% of summer days in the analyzed 1979 -2015 period. About half of these waves where associated with wave 7 (Tab. 3).

When scanning the data set for high amplitude events we detect 834 time steps in total (wave 6: 280, wave 7: 277, wave 8: 277). Of these events 237 fulfill conditions i. + ii. and pass the AT, corresponding to a ratio of 28 % (wave 6: 34%, wave 7: 37 %, wave 8: 15 %).

**Wave characteristics during QRA**

2D probability density distributions of phase speed and wave amplitudes were determined using a Kernel – density estimate for each of the conditions. These reveal that QRA episodes are characterized by high-amplitude waves at low phase speeds (Fig. 3). To test the influence of each of the conditions, we determine the probability density distributions under inclusion of conditions i., i.+ii. and i.+ii.+ AT separately. Fig. 3 shows the anomalies of probability-density distributions of phase speed and wave amplitudes of detected QRA days (coloured) compared to the 1979-2015 JJA climatology (black curves) for waves 6 - 8 (columns) and conditions i., i.+ii. and i.+ii.+AT (rows). The climatological spectrum (black curves) is dominated by eastward-traveling waves (positive phase speed) but features a fraction of quasi-stationary waves ( $c \approx \pm 2\ m/s$ ) and westward moving waves (negative phase speed) as well.

Under step-by-step inclusion of the different conditions, the detected days exhibit an increasing component of quasi-stationary high-amplitude waves (red), while the fraction of fast moving waves decreases (blue).

This is visible for all waves when condition i. and ii. are met: i.e. when a waveguide exists and the forcing is sufficient. For wave 7 high amplitude quasi-stationary waves are already much more frequent when only a waveguide is detected (condition i.). As expected applying the AT leads to a strengthening of the anomaly patterns detected for conditions i. +ii.

To test the significance of these findings, Fig. 4 compares amplitude distributions of quasi-stationary waves ( $-2\frac{m}{s} < c < 2\frac{m}{s}$) during QRA episodes (red line graph) and non-QRA episodes (black line graph). Distributions showing significant shifts (p - value < 0.05 in a Kolmogorov-Smirnov test) towards high amplitudes are marked with a red cross in the upper left corner (See Tab. A1 for exact values). For wave 7, episodes when waveguides are detected (condition i.) show a significant shift towards higher amplitudes already. Quasi-stationary components of both wave 6 and 7 show significant shifts towards higher amplitudes when the forcing condition (condition ii.) is added. Here, a small shift can be seen for wave 8 as well, however it is not significant (possibly also due to the much smaller sampling size for wave 8). After applying the Amplitude test, the shift towards high amplitudes becomes more pronounced for the distributions of all waves 6 – 8, but remains significant for wave 6 and 7 only.

These results confirm earlier findings (Petoukhov et al. 2013; Coumou et al. 2014) and provide quantitative statistics on all aspects of resonance by employing the postulated resonance conditions in an objective detection scheme. We detect a shift towards higher amplitudes for the quasi-stationary component of wave 6, 7 and 8 after applying the waveguide condition and the forcing condition only. For wave 6 and 7 these shifts are statistically significant.

In the next section we pursue these findings by analyzing circulation patterns of the longest QRA events detected.

**Mid-latitudinal circulation patterns and extremes during persistent QRA episodes**

For an evaluation of the circulation patterns during QRA episodes we analyzed long duration events (duration > 9 days) which gave rise to high-amplitude waves of at least 1.5 $\sigma$ above the 1979 – 2015 climatology during their occurrence (25 events in total). In the following we will analyze the 9 most prolonged episodes of which two exhibit simultaneous resonance events of two different wave numbers (Fig. 5a, 7a: 1994, and Fig. 5d, 7d: 2003) (see Tab. A2 for a complete list). Fig. 5 shows for each of these 9 episodes the time evolution of zonally averaged zonal wind, absolute value of the waves' phase speed $|c|$ and amplitude. Values are shown from 35 days before the first day of resonance to 35 days after the first resonance day. Events are ordered by the duration of the QRA-episode (indicated with a solid black horizontal bar) with the longest (1994) in the upper left and shortest in the lower right. Detected QRA periods are marked by a thick horizontal black line, which thus always starts at day “zero”. Calendar months are separated by dashed vertical lines and labeled at the bottom horizontal axis. Note that in August 1994 (Fig. 5a) and July 2003 (Fig. 5d) both wave 7 (upper black line) and wave 6 (lower black line) resonated. The phase speed of the respective wave is given in absolute values with low phase speeds ($|c| < 2.5$ m/s) shown in shades of red with step size of $0.5$ m/s. The respective 15 day running mean wave amplitude is given in units of standard deviation, where red denotes values above the $1.5\sigma$ threshold.

The majority of these prolonged QRA occurrences are wave 7 events and most events are found after the year 2000. Most of the depicted events share common characteristics: We identify (1) an emerging double jet (two distinct maxima in the zonally averaged zonal winds) prior to (2) QRA detection, which in turn precedes (3) the amplification of the respective wave. A probability density plot of the time step when the highest wave amplitude is reached has a maximum 6.3 days after the first day of resonance detection (Fig. 6), which is in good agreement with theory (Petoukhov et al. 2013; Feldstein 2000). The probability that the highest wave amplitude is reached after the first day of resonance detection is 80%.

In most cases the zonally averaged zonal wind is characterized by a strong subtropical jet positioned at latitudes around 45°N – 50°N. High amplitudes coincide with slow moving waves (c < 2 m/s). Exceptions are seen in August 2004 (Fig. 5e) and July 2001 (Fig. 5h) (both wave 7 events) where high wave amplitudes occur without slow wave progression.

The majority of detected periods coincide with extreme weather events in the NH caused by blocked or slow moving weather systems. Often those weather conditions occurred synchronous in different regions of the NH mid-latitudes. A link between resonance and individual extreme events can be found when analyzing the positions of North and Southward flow in the meridional wind fields during QRA events and the position of temperature anomalies (Fig. 7).

The meridional wind velocities (line contours) combined with temperature anomalies (coloured shading) in the mid-latitudes during those nine events are shown in Fig. 7 in the same order as in Fig. 5. Here, 15 day running mean wind fields are shown centered around the day within the QRA period exhibiting the highest wave amplitude.

Strongest meridional wind speeds are observed over North-America, the Atlantic and Western/Central Europe. The number of single waves (i.e. a pairs of Northward and subsequent Southward flow) fits the resonating wave in most cases, indicating that it is the most dominant wave. The temperature anomalies follow this alternating pattern, shifted by roughly half a wavelength: positive temperature anomalies are found between a Northward and a subsequent Southward flow, vice versa negative temperature anomalies are observed between pair of Southward and Northward flow.  This relationship is more pronounced in case of longitudinally confined and fast meridional wind-speeds. Consequently, as v-winds are strongest here, temperature anomalies are strongest over the western longitudes (-180°W – 50°E).

For comparison we show examples of situations without the QRA conditions fulfilled and moderate meridional wind speeds in Fig. A2 and Fig. A3. For completeness the azonal geopontential height fields in an analogue depiction during events shown in Fig. 5 are given in Fig. A1.

In the following we will shortly discuss the circulation patterns during each event while giving an account of concurrent reported extreme weather events in the NH mid-latitudes that might be linked to the observed high amplitude waves.

In summer 1994 QRA is detected for wave 6 and wave 7 during end of July /beginning of August (Fig 5a). During July – August the NH circulation was characterized by an above normal high pressure system over western Canada/Western United States, Europe and Japan causing abnormally warm conditions in those regions (Fig. A1a) (Halpert et al. 1995). In Europe the temperature anomalies were exceeding the 98% percentile and setting all time new maxima throughout central Europe (Halpert et al. 1995).A record setting heat wave over Korea and Japan lead to an excess death of 3000 in Korea (Kyselý & Kim 2009). The amplified meridional wind speeds triggered by QRA align with these temperature anomalies with warm anomalies in between pairs of Northward and Southward flow patterns (Fig. 7a).

In mid-June 1986 the jet splits, followed by QRA detection for wave 7 (Fig. 5b). A few days later the wave slows down and the amplitude increases sharply. The position of strong meridional wind speeds causes a split in temperature anomalies over North America with a hot West-coast and a cool East-side. The same wave pattern leads to positive temperature anomalies over Western Europe.

In June 2006 heat waves occurred over Europe (Rebetez et al. 2009), the US (Hoerling et al. 2007; Gershunov et al. 2009; Heim Jr. et al. 2007). The large scale circulation was characterized by strong meridional winds suggesting a strong meandering of the jet over Northern America, Europe and Asia (Fig. 7c). These events coincide with QRA detection for wave 7 which slows down and increased in amplitude soon after detection (Fig. 5c).

During the European heatwave in summer 2003 (Fig. 5d) we detect QRA for wave 7 and 6 from mid-July to beginning of August (see also Fig. 1). The amplified wave pattern stretched over the entire mid-latitudes of the NH causing synchronized anomalous weather in many places (Fig. 7d). In addition to the extraordinary conditions in Europe mentioned before (Fig. 1a-e), this led to very hot conditions in the eastern US and very wet and cold conditions in the West (Gleason et al. 2004), strong rains in China leading to severe flooding in the Huai River valley (Grover-Kopec 2004) and record breaking wet and cold conditions in Russia (Bulygin 2004).

A slow moving low pressure system brought above average precipitation to western Europe leading to the Bocastle (UK) floods in August 2004 (Golding et al. 2005). During the same time a persistent northwest flow over Northern America led to exceptionally low temperatures in central US (Bell 2005) and warm temperatures in western US (Fig. 7e). QRA is detected shortly after the jet splits and before the Amplitude of wave 7 reaches its peak during the first half of August (Fig. 5e). A view at the meridional wind patterns shown in Fig. 7e suggests that both events were connected by a hemispheric-wide persistent flow pattern. Wave speeds however don’t exhibit a distinct slowdown (Fig. 5e).

QRA conditions are met end of July of 2015, leading to above average wave amplitudes for wave 7 and decelerated wave speeds throughout August (Fig. 5f). A persistent ridge over Eurasia led to pronounced heat in Central to Eastern Europe and the continuation of the heatwave that started in June (German Weather Service 2015). This temperature anomaly is also visible in Fig. 7f. We note that no double jet pattern in $U$ is observed during the first half of the QRA event.

In 2009 we detect resonance for wave 8 by the end of June with wave amplitudes peaking a few days later. Wave speeds slow down, but exhibit total values below 1.5 m/s for a short time only. No double jet pattern is observed (Fig. 5g). Heat anomalies are observed in North-West America, Western Europe and Western Eurasia (Fig. 7g).

In July 2001 a persistent meridional flow pattern over North America caused a heatwave in the central US and cold temperatures over the East and West coast (NOAA National Climatic Data Center 2001) (Fig. 7h). This is reflected by a high-amplitude wave 7 (Fig. 5h) and strong meridional winds over most of the hemisphere, especially and most intensely over the US (Fig. 7h). QRA conditions are met about two weeks prior to the observation of the maximum amplitude (Fig. 5h).

In 1985, QRA is first detected for wave 7 by late June followed by a rise in this wave’s amplitude (Fig. 5i) and a slowdown in phase speed. High-amplitude meridional wind speeds are observed most notably over the Pacific and the US. Positive temperature anomalies are found at the US West-Coast, Western Europe and China (Fig. 7i).

**Mid-latitude Extreme Index**

The prolonged resonance events shown in figures 5 and 7 thus were predominantly associated with documented extremes. Here we assess the statistical relationship between QRA events and weather extremes by applying the MEX-index (*Mid-latitudinal Extreme Index*, see Methods). This index provides a measure of hemispheric synchronization of extremes in the mid-latitudes allowing for a quantitative comparison of QRA events and non-events (Coumou et al. 2014). We calculate the MEX index based on daily temperature anomalies and compare QRA and Non-QRA days by comparing their MEX- probability density function (Fig. 8).

We find an increased tendency for hot extremes during QRA events (Fig. 8). The distributions during QRA are shifted towards more extremes compared to non QRA-days. A statistically significant shift ($p < 0.05$, based on a Kolmogorov-Smirnov test) is found when focusing on persistent events (duration > 14 days) (Fig. 8). The relationship between QRA and rainfall, however cannot be confirmed by this statistic approach (not shown), even though single extreme rainfall events were shown to be linked to QRA (Stadtherr et al. 2016). There are several potential reasons for this. Rainfall extremes are much more local and short lived compared to the large scale temperature anomalies discussed here. Furthermore, available reanalysis data is noisier and less reliable for precipitation then for temperatures. Additionally, QRA is expected to be important for frontal precipitation only, while having no effect on the occurrence of other mechanisms like convective or orographic precipitation.

## IV. Discussion

Seven out of nine major QRA events detected have been found to be connected with a double jet pattern in the zonally averaged zonal wind (Fig. 5), consistent with results of previous studies (Petoukhov et al. 2013; Coumou et al. 2014). Tachibana et al. (2010) found a double jet stream structure in summer to be associated with blocking and a positive northern annular mode (NAM). From a geographic perspective (rather than the zonal mean), a persistent split in the jet stream over a range of longitudes (potentially leading to a double jet in the zonal mean) serves as a key indicator for blocking events (Rex 1950; Barriopedro et al. 2010). Most of these phenomena associated with double jet structures share anomalous surface weather in the mid-latitudes as an outcome. For the nine most prolonged resonance events detected (Fig. 5) there appears to be a typical sequence of events: From (1) formation of a double jet (two peaks in the zonal mean zonal wind) to (2) first QRA detection, to (3) amplified waves with relatively low zonal phase speeds. The latter is also shown to be statistically significant for wave 6 & wave 7 resonance events (Fig. 4).

Not all events presented in Fig. 5 follow this specific sequence. In 2003 (wave 7, Fig5.d) and 2001 (wave 7, Fig. 5h) high amplitude waves emerge *before* QRA-detection. In 2004 (Fig. 5a) and 2009 (Fig. 5g) amplitudes are already above average and exceed the $1.5\ \sigma$ level very shortly after QRA is detected. Still, in all cases amplitudes rise again *after* QRA conditions are met. Clearly, QRA is not the only mechanism that can generate waves of high amplitude, explaining why high amplitude waves can occur before resonance detection. Also, the simplified resonance equations exclude non-linear mechanisms which might be important during individual events. Therefore, the exact sequence might be somewhat different in individual events, but, more importantly, the chance for high-amplitude waves is much higher in the two weeks directly after first resonance detection. The double jet pattern emerges approximately 1-2 weeks prior to first QRA detection, which in turn leads the observation of amplified waves by approximately one week (Fig. 6). This suggests that a double jet structure in the zonal mean favors waveguide formation and hence resonance to occur.

However, the event presented in Fig. 5f and Fig. 5g illustrates that it is the shape of jet which is vital for waveguide formation (Petoukhov et al. 2013) and that waveguides typically form around a latitude of 40° (Fig. 1c , Fig. 1h). A strong and narrow jet leads to a second turning point on the subtropical flank complementing the turning point on the poleward flank. Our results suggest that this characteristic shape is more likely to occur during double jets in the zonal average.

It has been shown that double jet structures are caused by strong step-like gradients in the PV-field  (Martius et al. 2010). This could indicate that a double jet is associated with a sharper subtropical jet situated further South compared to a single jet state, which in turn favors the formation of a waveguide.

Hoskins & Karoly (1981) introduced a concept of quasi-stationary wave trains, defined as those wave patterns whose wave action (proportional to energy) propagates along rays with local group velocity as a function of the zonal wavenumber $k$ and the meridional wavenumber $l$. Here, $k$ is constant along the ray, and $l$ varies along the ray so that the sum of $k^2$ and $l^2$ equals the square of the stationary wave number $K_S$ (which is a function of the zonal wind). The waveguides for these wave trains are confined by two turning points on which $l^2$ crosses zero, with the condition that $l^2 > 0$ in between (see Tab.1).

Thus, in the framework of the QRA hypothesis, the latitudinal shape of the zonally averaged zonal wind is a central measure for characterizing the state of the quasi-stationary wave circulation patterns in the mid-latitudes. Also, with the zonally averaged zonal winds given (i.e. taken from observations), the QRA hypothesis can only be used as a diagnostic, and not a predictive, tool for the study of wave resonance events. This approximation to real world processes leads to two limitations of the hypothesis in its current form. Firstly, in this zonal mean representation we neglect regional variations in the zonal flow and refractive indices. Likewise, the QRA – mechanism does not provide information on the location of an individual extreme event, but rather serves as a physical explanation for the occurrence of high amplitude waves. Secondly, by following the zonal mean approach, meridionally oriented waveguides are explicitly excluded from the analysis. Consequently, the QRA – mechanism describes waves that move in the zonal direction.

However, the approximations made, enable an analytical derivation of resonance equations and thus provide physical understanding, and as usual in physics they are motivated by empirical observations: The recently observed circulation patterns, which we aim to explain, were firstly *hemisphere - wide* and secondly *zonal* in nature: Chains of zonally elongated stationary wave trains of high amplitudes stretched over the entire hemisphere leading to a number of extreme weather events in recent years in the NH.

## V.Conclusion

By casting the conditions for the amplification of quasi-stationary waves (QRA) as postulated by Petoukhov et al. (2013) into a detection scheme, we established an objective method to scan large datasets for QRA events. Applied on reanalysis data (1979 -2015) the scheme reveals that during about one-third of all high amplitude events (> 1.5 σ) for waves 6, 7, 8 the QRA conditions are met. Spectral analysis of QRA events shows an increased component of slow-moving high-amplitude waves as compared to summer climatology. For wave 6 and wave 7 this shift in wave characteristics is statistically significant, where wave 8 shows the same tendency without a statistical significance. These results provide evidence for the validity of the hypothesis and its underlying assumptions.

Analyzing the most persistent high amplitude QRA events we find that QRA detection precedes the maximum wave amplitude by about a week. Many of the detected events were associated with a double jet visible in the zonally averaged zonal wind. Anomalous hemispheric wide weather conditions occurred during the majority of the QRA periods presented here and we provide statistical evidence that QRA events lead to surface extremes. Our results suggest that those events were linked to stationary waves with high amplitudes stretching over the mid-latitudes. QRA periods coincide with wave amplification and therefore the alignment of meridional wind velocities (i.e. reduction in phase speed). A cluster of prolonged resonance is found after 2000 with 6 out of 9 events occurring after 2000 (though its significance is unclear), many of those coincide with NH mid-latitude weather extremes. This cluster was primarily due to long lasting wave 7 resonance events.

Extreme surface weather events occurred predominantly in the regions near strong meridional winds. Still, amplified waves (or more specifically resonance) alone do not necessarily lead to extremes, but they create favorable conditions for extremes to occur(Screen & Simmonds 2014). By generating hemispheric wide quasi-stationary high-amplitude waves, QRA is setting the stage on which extreme weather is more probable. Factors like wave phase (setting of ridges and troughs), soil moisture (Miralles et al. 2014) and synoptic weather conditions can turn prolonged weather conditions into extremes.

To further investigate this relation, future work will head towards further analyzing the interplay of double jet structures, QRA and extreme weather events.

Furthermore, this operational QRA detection scheme enables us to explore the representation of the QRA-mechanism in climate models. By applying the scheme to climate model output (e.g. CMIP5) statistical analyses of QRA events under future projections of different climate scenarios can be done. Whether CMIP5 models can accurately reproduce resonance events is of particular interest considering that models have known biases related to summer Rossby wave activity (Schubert et al. 2011). The detection scheme also serves as a first step towards an improved understanding of the underlying drivers. To further explore the QRA mechanism and its role in the generation of weather extremes, the detection scheme will be applied to the southern hemisphere. Australia recently experienced a set of extreme weather events, including extreme precipitation and drought events which require an explanation and QRA could be a potential candidate.

## VII. Acknowledgements

We thank the NCEP/NCAR Reanalysis Project at the NOAA/ESRL Physical Sciences Division for making their data available. The presented work was supported by the German Federal Ministry of Education and Research (grant no. 01LN1304A). We also gratefully acknowledge the European Regional Development Fund (ERDF), the German Federal Ministry of Education and Research (BMBF) and the Land Brandenburg for supporting this project by providing resources on the high performance computer system at the Potsdam Institute for Climate Impact Research. We thank two anonymous reviewers for their comments which much improved this manuscript.

## VIII. References

Ambrizzi, T., Hoskins, B.J. & Hsu, H.-H., 1995. Rossby Wave Propagation and Teleconnection Patterns in the Austral Winter. *Journal of the Atmospheric Sciences*, 52(21), pp.3661–3672.

Archer, C.L. & Caldeira, K., 2008. Historical trends in the jet streams. *Geophysical Research Letters*, 35(8), p.L08803.

Barriopedro, D., García-Herrera, R. & Trigo, R.M., 2010. Application of blocking diagnosis methods to General Circulation Models. Part I: a novel detection scheme. *Climate Dynamics*, 35(7-8), pp.1373–1391.

Bell, G.D., 2005. April- July 2004: Hot in Alaska and Yukon, Cool in Central North America in: State of the Climate in 2004. *Bull. Amer. Meteor. Soc.*, pp.46–47.

Black, E. et al., 2004. Factors contributing to the summer 2003 European heatwave. *Weather*, 59(8), pp.217–223.

Bulygin, O.N., 2004. Russia in State of the Climate 2003. *Bull. Amer. Meteor. Soc.*, 85, pp.55– 57.

Charney, J.G. & Eliassen, A., 1949. A Numerical Method for Predicting the Perturbations of the Middle Latitude Westerlies. *Tellus*, 1(2), pp.38–54.

Christidis, N., Jones, G.S. & Stott, P. a., 2014. Dramatically increasing chance of extremely hot summers since the 2003 European heatwave. *Nature Climate Change*, (December), pp.3–7.

Coumou, D. et al., 2014. Quasi-resonant circulation regimes and hemispheric synchronization of extreme weather in boreal summer. *Proceedings of the National Academy of Sciences*, 111(34), pp.12331–12336.

Coumou, D., Lehmann, J. & Beckmann, J., 2015. The weakening summer circulation in the Northern Hemisphere mid-latitudes. *Science*, 348(6232), pp.324–327.

Coumou, D. & Rahmstorf, S., 2012. A decade of weather extremes. *Nature Climate Change*, 2(7), pp.1–6.

Coumou, D. & Robinson, A., 2013. Historic and future increase in the global land area affected by monthly heat extremes. *Environmental Research Letters*, 8(3), p.034018.

Coumou, D., Robinson, A. & Rahmstorf, S., 2013. Global increase in record-breaking monthly-mean temperatures. *Climatic Change*, 118(3-4), pp.771–782.

Dickinson, R.E., 1970. Development of a Rossby Wave Critical Level. *Journal of Atmospheric Sciences*, 27, pp.627–633.

Dingle, R.B., 1973. *Asymptotic Expansions: Their derivation and interpretation*, London, New York: Academic Press.

Dole, R. et al., 2011. Was there a basis for anticipating the 2010 Russian heat wave? *Geophysical Research Letters*, 38(January), pp.1–5.

Feldstein, S.B., 2000. Teleconnections and {ENSO}: the timescale, power spectra, and climate noise properties. *J. Clim.*, 13, pp.4430–4440.

Fischer, E.M. & Knutti, R., 2015. Anthropogenic contribution to global occurrence of heavy-precipitation and high-temperature extremes. *Nature Climate Change*, 5(April), pp.1–6.

German Weather Service, 2015. Monthly event calendar. *for the year: 2015 and the month: August*.

Gershunov, A., Cayan, D.R. & Iacobellis, S.F., 2009. The great 2006 heat wave over California and Nevada: Signal of an increasing trend. *Journal of Climate*, 22(23), pp.6181–6203.

Gleason, K.L. et al., 2004. United States in State of the Climate in 2003. *Bulletin of the American Meteorological Society*, 85, pp.36 –41.

Golding, B., Clark, P. & May, B., 2005. The Boscastle flood: Meteorological analysis of the conditions leading to flooding on 16 August 2004. *Weather*, 60(8), pp.230–235.

Grover-Kopec, E.K., 2004. China in State of the Climate 2003. *Bulletin of the American Meteorological Society*, 85, pp.53 – 54.

Halpert, M.S. et al., 1995. State of the Climate in 1994. *Bull. Amer. Meteor*.

Hansen, J., Sato, M. & Ruedy, R., 2012. Perception of climate change. *Proceedings of the National Academy of Sciences of the United States of America*, 109(37), pp.E2415–23.

Hastings, D. & Dunbar, P., 1999. Global land one-kilometer base elevation (GLOBE) digital elevation model. *Documentation, Key to Geophysical Records Documentation*, 1.0.

Heim Jr., R.. et al., 2007. United States in: State of the Climate in 2006. *Bulletin of the American Meteorological Society*, 88(84-87).

Hoerling, M. et al., 2007. Explaining the record US warmth of 2006. *Geophysical Research Letters*, 34(17), pp.1–4.

Horton, D.E. et al., 2015. Contribution of changes in atmospheric circulation patterns to extreme temperature trends. *Nature*, 522(7557), pp.465–469.

Hoskins, B.J. & Ambrizzi, T., 1993. Rossby Wave Propagation on a Realistic Longitudinally Varying Flow. *Journal of the Atmospheric Sciences*, 50(12), pp.1661–1671.

Hoskins, B.J. & Karoly, D.J., 1981. The Steady Linear Response of a Spherical Atmosphere to Thermal and Orographic Forcing. *Journal of the Atmospheric Sciences*, 38, pp.1179–1196.

IPCC, 2012. *Managing the Risks of Extreme Events and Disasters to Advance Climate Change Adaptation* C. B. Field et al., eds., Cambridge, UK, and New York, NY,USA: Cambridge University Press.

Kalnay, 1996. The NCEP/NCAR 40-year reanalysis project. *Bulletin of the American Meteorological Society*, (77), pp.437–470.

Kyselý, J. & Kim, J., 2009. Mortality during heat waves in South Korea, 1991 to 2005: How exceptional was the 1994 heat wave? *Climate Research*, 38(2), pp.105–116.

Lau, W.K.M. & Kim, K.-M., 2012. The 2010 Pakistan Flood and Russian Heat Wave: Teleconnection of Hydrometeorological Extremes. *Journal of Hydrometeorology*, 13(1), pp.392–403.

Lehmann, J., Coumou, D. & Frieler, K., 2015. Increased record-breaking precipitation events under global warming. *Climatic Change*, 132(4), pp.501–515.

Luterbacher, J. et al., 2004. European Seasonal and Annual Temperature Variability, Trends, and Extremes Since 1500. *Science*, 303(5663), pp.1499–1503.

Martius, O., Schwierz, C. & Davies, H.C., 2010. Tropopause-Level Waveguides. *Journal of the Atmospheric Sciences*, 67(3), pp.866–879.

Min, S.-K. et al., 2011. Human contribution to more-intense precipitation extremes. *Nature*, 470(7334), pp.378–81.

Miralles, D.G. et al., 2014. Mega-heatwave temperatures due to combined soil desiccation and atmospheric heat accumulationle. *Nature Geoscience*, 7, pp.345–349.

Murdock, J.A., 1987. *Perturbations: Theory and Methods (Classics in Applied Mathematics)*, Society for Industrial and Applied Mathematics.

NOAA National Climatic Data Center, 2001. *2001 Summer Heat in the United States*, Asheville NC.

Ogi, M., Yamazaki, K. & Tachibana, Y., 2005. The summer northern annular mode and abnormal summer weather in 2003. *Geophysical Research Letters*, 32(4), pp.1–4.

Olver, F.W.J., 1975. Second-Order Linear Differential Equations with Two Turning Points. *Philosophical Transactions A*, 278(1279), pp.137–174.

Overland, J.E. et al., 2012. The recent shift in early summer Arctic atmospheric circulation. *Geophysical Research Letters*, 39(19), pp.1–6.

Palmer, T.N., 2013. Climate extremes and the role of dynamics. *Proceedings of the National Academy of Sciences of the United States of America*, 110(14), pp.5281–2.

Pedlosky, J., 1979. *Geophysical Fluid Dynamics*, New York, Heidelberg, Berlin: Springer-Verlag.

Petoukhov, V. et al., 2013. Quasiresonant amplification of planetary waves and recent Northern Hemisphere weather extremes. *Proceedings of the National Academy of Sciences of the United States of America*, 110(14), pp.5336–41.

Petoukhov, V. et al., 2016. The role of quasi-resonant planetary wave dynamics in recent boreal spring-to-autumn extreme events. *Proceedings of the National Academy of Sciences*, 113(25), pp.6862 – 6867.

Rahmstorf, S. & Coumou, D., 2011. Increase of extreme events in a warming world. *Proceedings of the National Academy of Sciences of the United States of America*, 108(44), pp.17905–9.

Rebetez, M., Dupont, O. & Giroud, M., 2009. An analysis of the July 2006 heatwave extent in Europe compared to the record year of 2003. *Theoretical and Applied Climatology*, 95(1-2), pp.1–7.

Rex, D.F., 1950. Blocking Action in the Middle Troposphere and its Effect upon Regional Climate. *University of Stockholm*.

Russo, S. et al., 2014. Magnitude of extreme heat waves in present climate and their projection in a warming world. *Journal of Geophysical Research: Atmospheres*, p.n/a–n/a.

Schär, C. et al., 2004. The role of increasing temperature variability in European summer heatwaves. *Nature*, 427(January), pp.3926–3928.

Schneider, T., Bischoff, T. & Płotka, H., 2014. Physics of changes in synoptic midlatitude temperature variability. *Journal of Climate*, 28, pp.2312–2331.

Schubert, S., Wang, H. & Suarez, M., 2011. Warm Season Subseasonal Variability and Climate Extremes in the Northern Hemisphere: The Role of Stationary Rossby Waves. *Journal of Climate*, 24(18), pp.4773–4792.

Screen, J.A. & Simmonds, I., 2014. Amplified mid-latitude planetary waves favour particular regional weather extremes. *Nature Climate Change*, 4(8), pp.704–709.

Stadtherr, L. et al., 2016. Record Balkan floods of 2014 linked to planetary wave resonance. *Science Advances*, (April), p.(minor revisions).

Tachibana, Y. et al., 2010. Abrupt evolution of the summer Northern Hemisphere annular mode and its association with blocking. *Journal of Geophysical Research*, 115(D12), p.D12125.

Tung, K.K. & Lindzen, R.S., 1979. A Theory of Stationary Long Waves. Part I: A Simple Theory of Blocking. *Monthly Weather Review*, 107, pp.714–734.

Westra, S., Alexander, L. V. & Zwiers, F.W., 2013. Global Increasing Trends in Annual Maximum Daily Precipitation. *Journal of Climate*, 26(11), pp.3904–3918.

## IX. Tables

i. *Waveguide for synoptic scale free wave k:*

1. Two turning points (TPs, change of sign) in $l^2$
2. $l^2 > 0$ between the turning points (TP)
3. $U > 0$ in between and in the vicinity of the TPs
4. The highest value of $l^2$ between the TPs is in the range of $l^2_{min}$ and $l^2_{max}$
5. The TPs lie within a region of 30°N and 70°N
6. The TPs have a minimum distance of $w_k$
7. In case of two waveguides their distance has to exceed at least 5°

ii. *Effective Forcing Amplitude for forced wave $m \approx k$:*

8. The effective forcing Amplitude $A_{eff}$ for a respective wave number $m$ has to exceed a certain threshold $q_k$.

**Tab. 1:** *Overview of applied QRA detection conditions* i.-ii.

| *Condition/Wave* | *Wave 6*<br><br>*Events/days* | *Wave 7*<br><br>*Events/days* | *Wave 8*<br><br>*Events/days* | *Total*<br><br>*Events/days* |
|---|---|---|---|---|
| i | *126/839* | *115/935* | *77/480* | *318/2254* |
| i+ii | *112/572* | *116/915* | *80/420* | *308/1907* |
| i+ii+AT | *94/495* | *54/503* | *30/187* | *143/1185* |

**Tab. 2:** : *Number of detected events per condition and no. of corresponding 15 – day running mean days. By 'splitting' longer events in to several parts condition ii leads to an increase in number of events.*

| *Condition/Wave* | *Wave 6*<br>*Events/days* | *Wave 7*<br>*Events/days* | *Wave 8*<br>*Events/days* | *Total*<br>*Events/days* |
|---|---|---|---|---|
| i | *34/542* | *36/656* | *19/297* | *89/1495* |
| i+ii | *19/280* | *35/628* | *16/241* | *70/1149* |
| i+ii+AT | *17/257* | *22/387* | *8/116* | *47/760* |

**Tab.3:** *Number of detected events exceeding a minimum duration of 10 timesteps, listed by condition and no. of corresponding 15 – day running mean days.*

## X. Figures

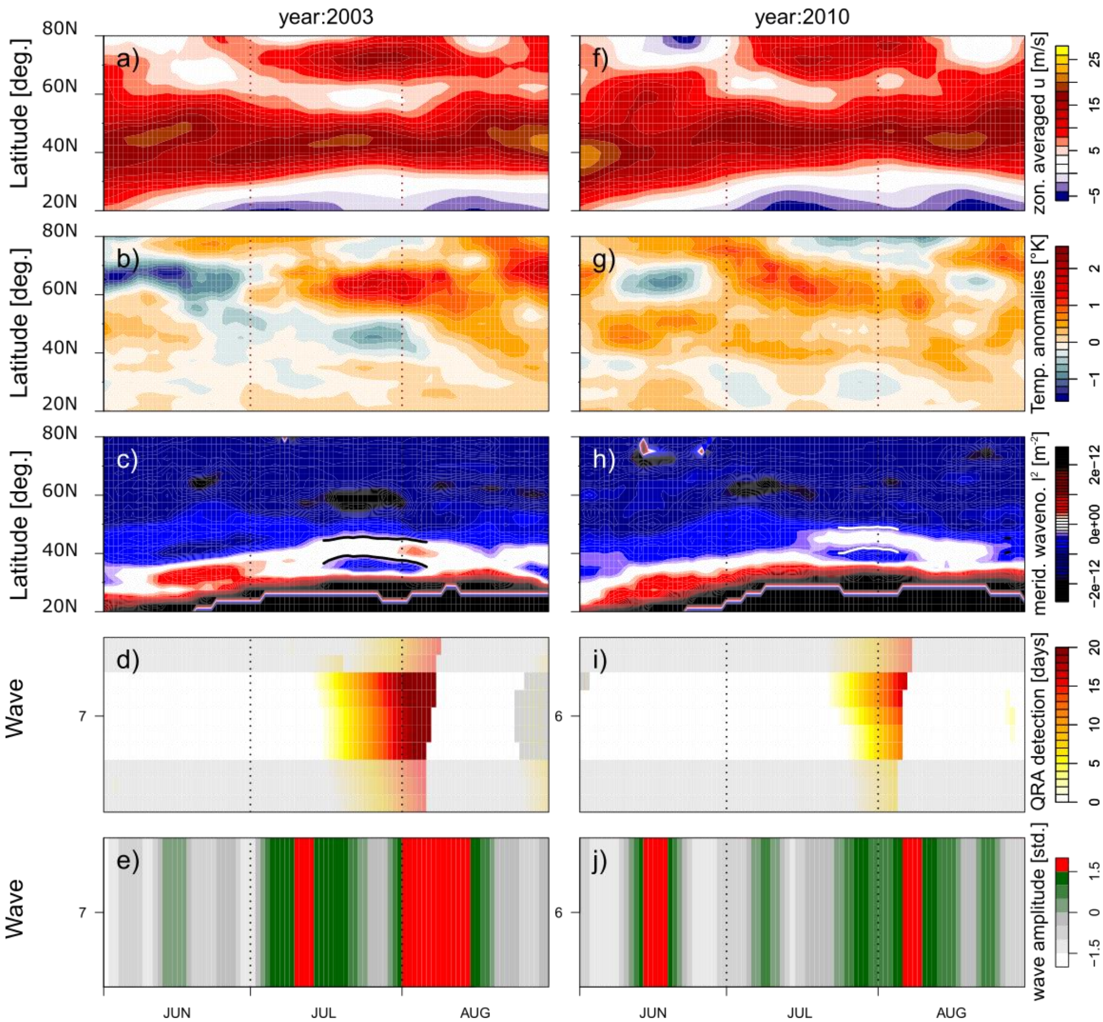


**Fig. 1:** *QRA case studies of summer months (JJA) of 2003 European heatwave (a-e) and 2010 Moscow heatwave (f-j). Sub-figures show Hovmöller plots of the zonally averaged zonal wind (a,*

*f), zonally averaged temperature anomalies (b, g) and meridional wave number $l^2$ (c, h). Here the black (white in h) lines mark the waveguides' turning points (solid for wave 7 and dashed for wave 6). QRA detection for k=5.5, 5.6, …, 8.4 is shown in Sub-plots (d, i). The relevant areas for resonance ($k = m \pm 0.2$ with $m = 6{,}7{,}8$) are shown in colors of higher saturation. The color scale illustrates the number of consecutive resonance days meeting the QRA conditions. Days/wave numbers fulfilling conditions i.) and ii.) but failing the AT are masked in grey. In e, j) amplitudes of the meridional NH-midlatitudinal wind field of wave 6, 7, 8 are shown in units of standard deviation with respect to the seasonal (JJA) climatological mean. Amplitudes exceeding a standard deviation of $\sigma = 1.5$ are shown in red.*

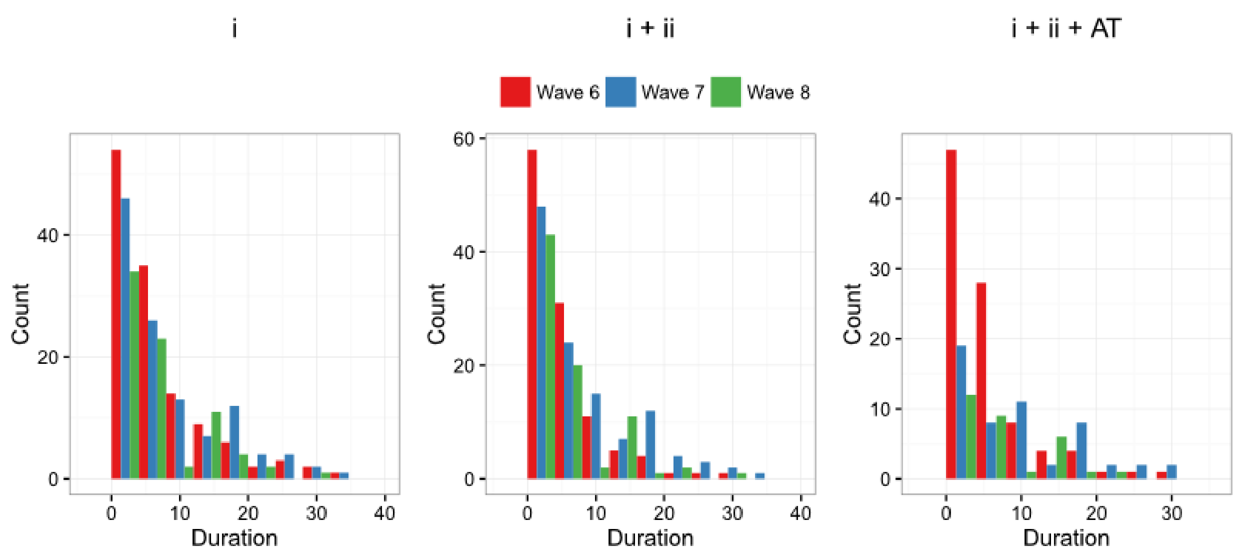


**Fig. 2:** *Distribution of duration of detected episodes for condition i, ii and after applying the AT for waves 6, 7 and 8. The bin width was set to 4. The majority of detected events are smaller than 8 days.*

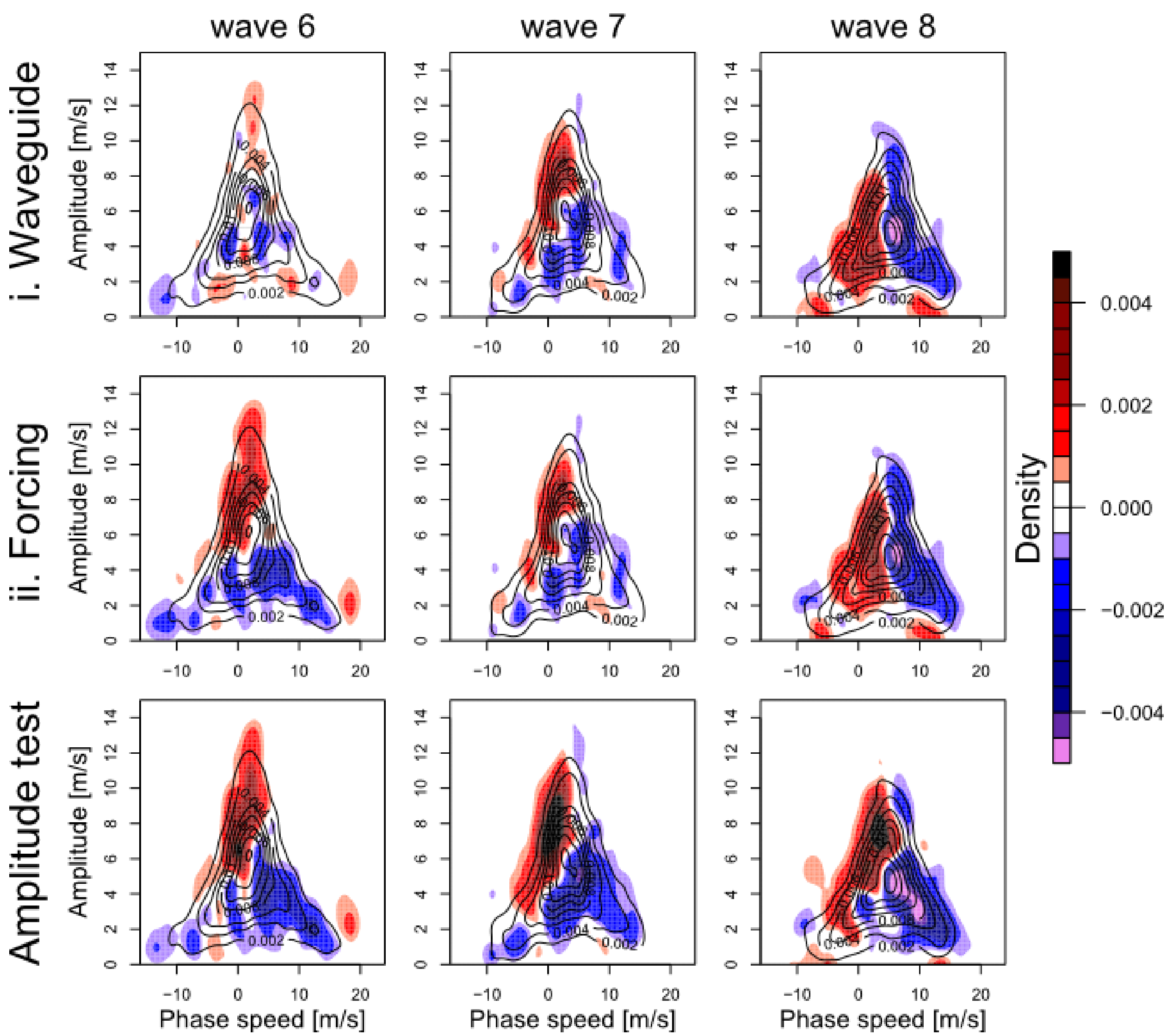


**Fig. 3:** *Anomalies of probability density distributions of wave speed vs. wave amplitude during detected QRA events for waves 6 (left column), 7 (middle column), 8 (right column) after applying conditions i. (top row), i.+ii. (middle row) and i.+ii.+ AT (bottom row). Anomalies are shown in colored contours on top of JJA climatology* (black solid curves). *Positive anomalies (red) are observed in the area of slow moving high-amplitude waves for detected QRA-days, while the density of low amplitude fast waves is reduced (blue).*

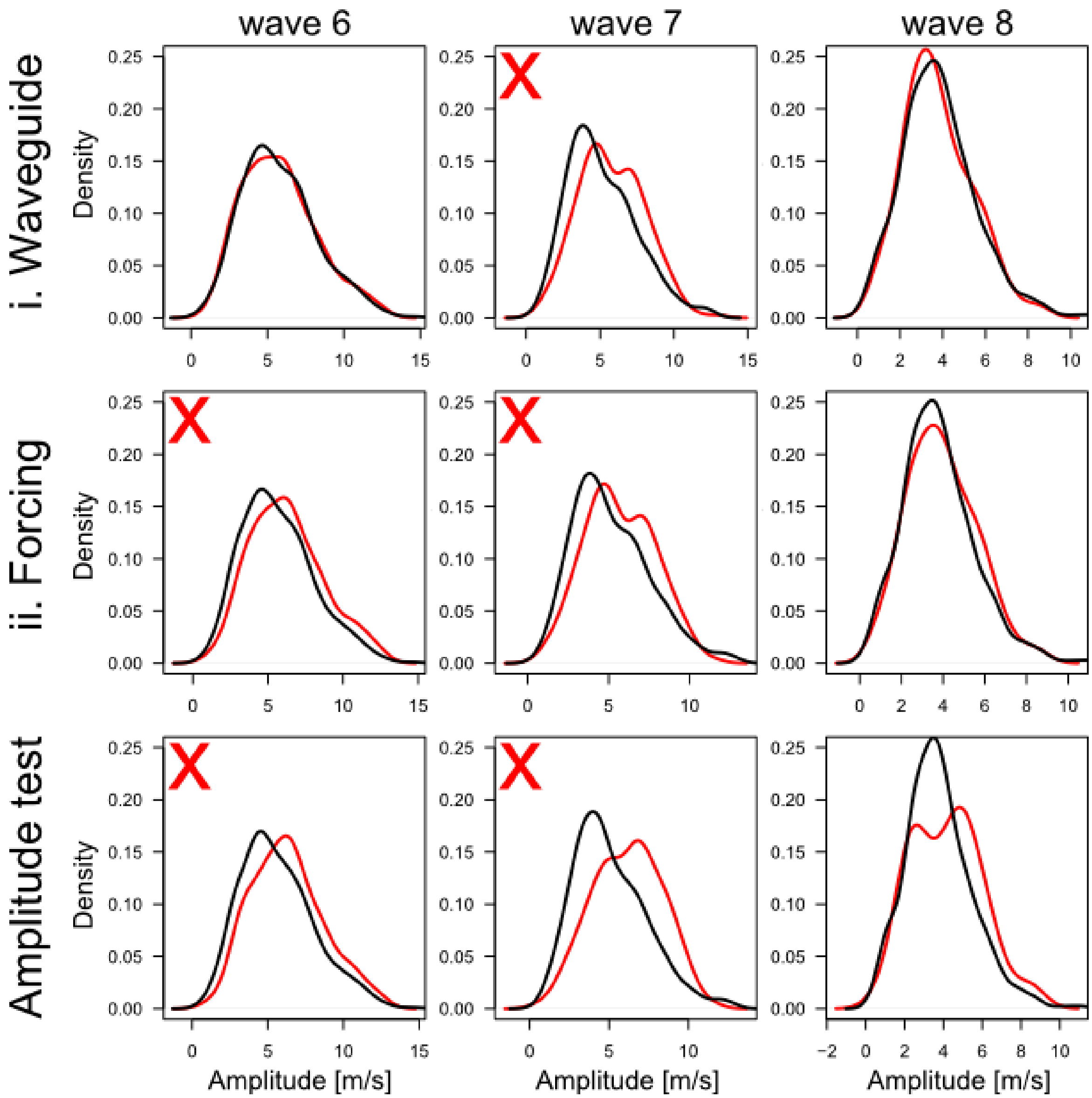


**Fig. 4:** *Probability density distribution of amplitudes of quasi-stationary waves ($c = \pm 2\ m/s$) at 300 mb of days detected when applying conditions i., i.+ii and i.+ii.+ AT rows) of wave 6, 7, 8 (columns) during 1979 – 2014 summer (red) compared to days when respective conditions were not met (black). Except for the pairing condition i./wave 8 (upper right) an overall shift in the distribution towards higher amplitudes is observed. Subplots marked with a red 'X' show statistically significant shifts (see Appendix, Table S1).*

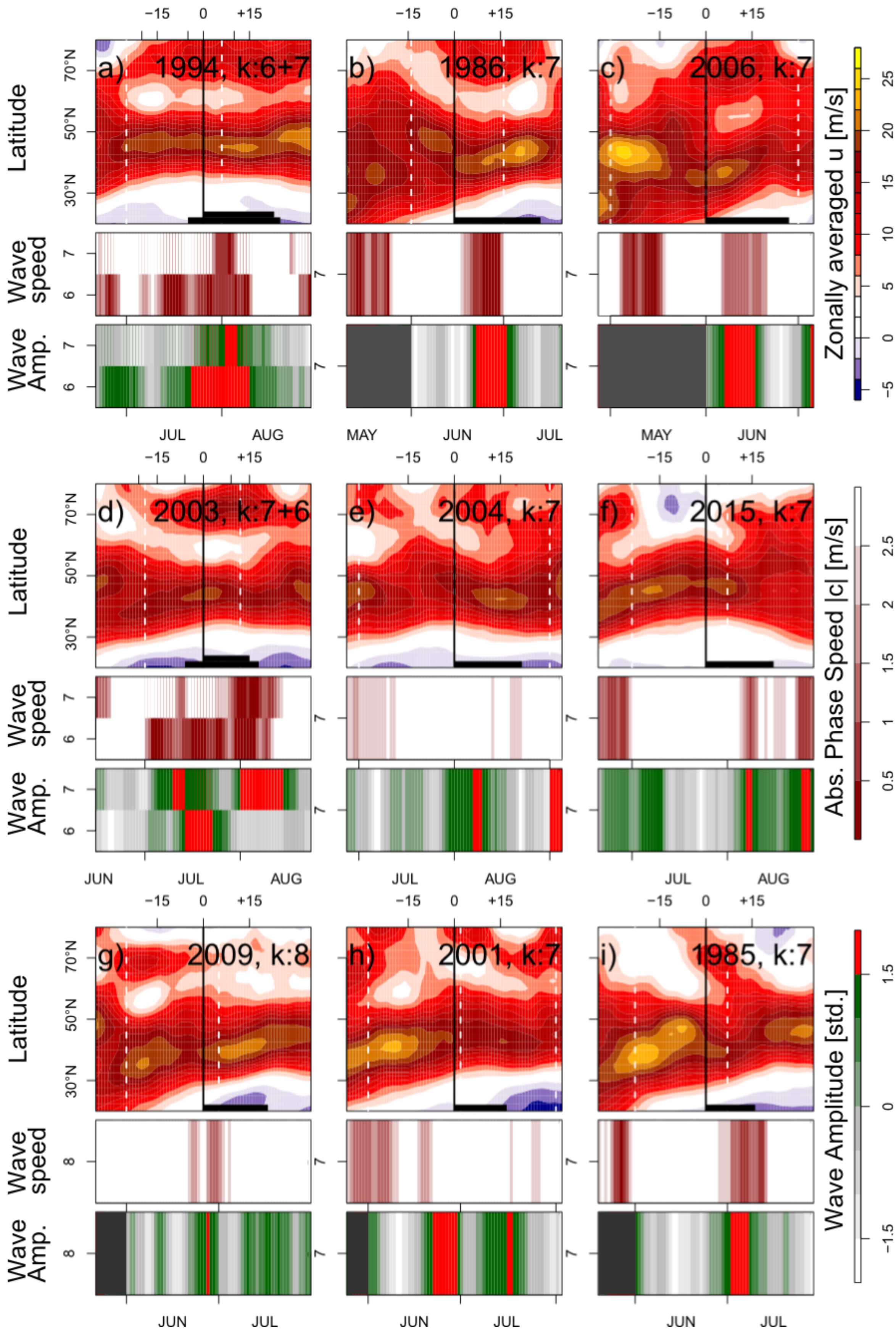
a) 1994, k:6+7
b) 1986, k:7
c) 2006, k:7
d) 2003, k:7+6
e) 2004, k:7
f) 2015, k:7
g) 2009, k:8
h) 2001, k:7
i) 1985, k:7
−15
0
+15
Latitude
70°N
50°N
30°N
Wave speed
Wave Amp.
MAY
JUN
JUL
AUG
Zonally averaged u [m/s]
Abs. Phase Speed |c| [m/s]
Wave Amplitude [std.]

**Fig. 5:** *Hovmöller plots of zonally averaged zonal wind, phase speed as absolute values and respective wave amplitudes during the nine longest detected resonance episodes that coincide with observed wave amplitudes above 1.5σ of the climatology. Wave amplitudes are given in units of standard deviation from JJA climatology. Therefore no values are given for May and September (dark grey). The subfigures are aligned in time by the first resonance day (day "0", marked with a solid vertical black line), while giving a 35 days lead and lag period. The detected QRA periods and their durations are marked with horizontal solid black lines at the bottom. Vertical dashed lines are marking the months. The majority of events are wave 7 events falling in the period after year 2000. QRA is often associated with a double jet pattern in the zonally averaged zonal wind.*

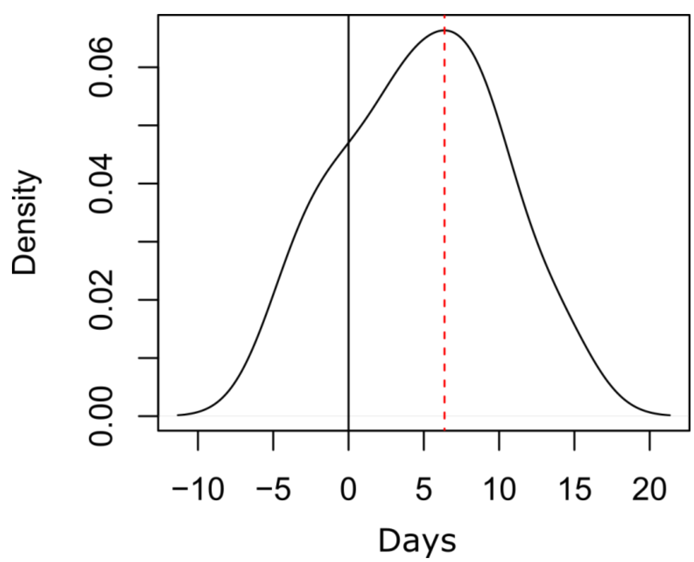


**Fig. 6:** *Probability density of lead lag times of a maximum amplitude within a window of* $\pm 14$ *days relative to the first day of QRA detection ('day 0'). Only long duration events coinciding with a wave amplitude of <1.5σ are included (25 events). A maximum (marked with a red dashed line) is observed at a time lag of about 6 days.*

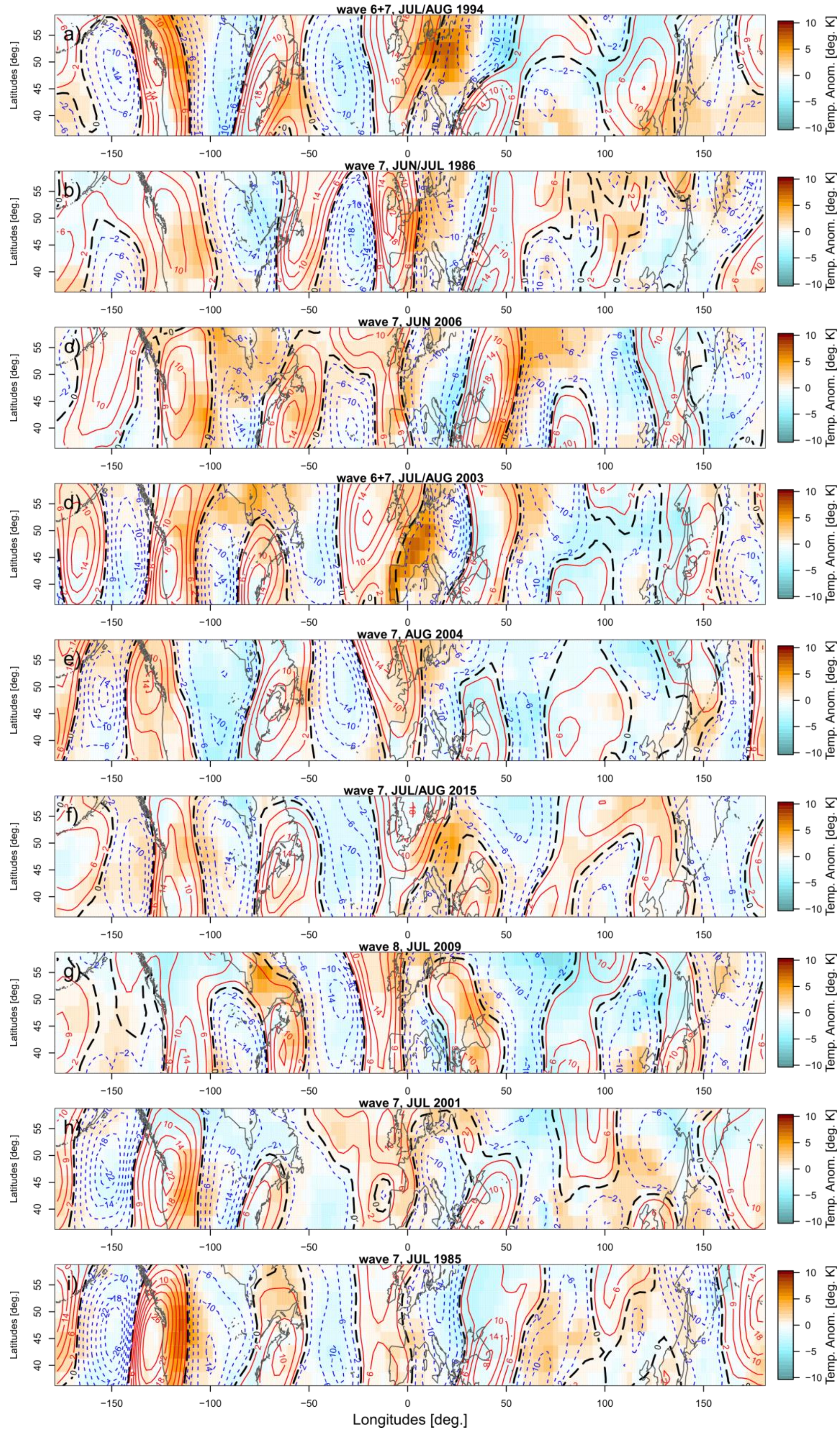
wave 6+7, JUL/AUG 1994
wave 7, JUN/JUL 1986
wave 7, JUN 2006
wave 6+7, JUL/AUG 2003
wave 7, AUG 2004
wave 7, JUL/AUG 2015
wave 8, JUL 2009
wave 7, JUL 2001
wave 7, JUL 1985
a)
b)
d)
d)
e)
f)
g)
h)
i)
Latitudes [deg.]
Temp. Anom. [deg. K]
Longitudes [deg.]

**Fig. 7:** *15 day running mean meridional wind fields (line contours, South - North: blue, dashed, North - South: red, zero-line: black, long-dashed) and 15 day running mean temperature anomalies (color shading) of the NH mid-latitudes during the nine longest resonance episodes detected (as in Fig. 5 and Tab. A2). Wind velocities and temperature anomalies are averaged over the 15 days centered on the day with the highest wave amplitude within the respective QRA period. Landmass is depicted in dark grey by the respective coastlines.*

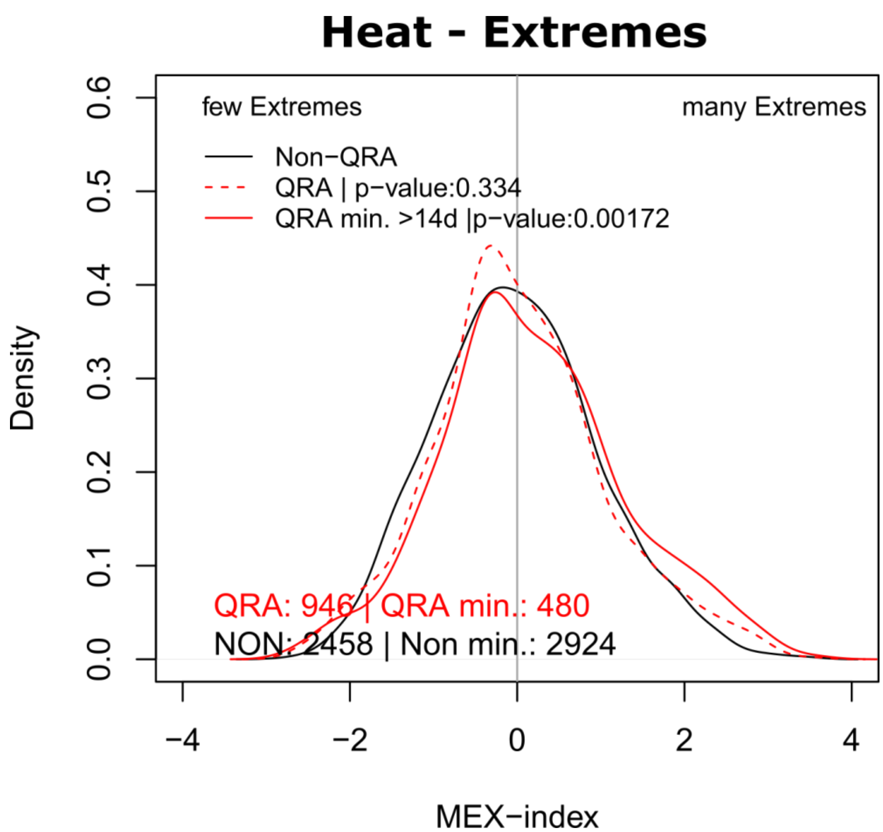


**Fig. 8**: *Probability density plots of MEX-index derived from daily temperature anomaly fields. Densities are shown for all QRA events of wave 6 – 8 (red dashed line) and QRA events of wave 6 – 8 of a minimum duration of 14 (red solid line) in comparison with Non – QRA days. The ensemble size is given in the lower left corner. Long QRA events show an increase in daily heat extremes, while there doesn't seem to be a relation between precipitation and QRA.*

## X. Captions

**Tab. 1:** *Overview of applied QRA detection conditions* i.-ii.

**Tab. 2**: *Number of detected events per condition and no. of corresponding 15 – day running mean days. By 'splitting' longer events in to several parts condition ii leads to an increase in number of events.*

**Tab. 3:** *Number of detected events exceeding a minimum duration of 10 per condition and no. of corresponding 15 – day running mean days.*

**Fig. 1:** *QRA case studies of summer months (JJA) of 2003 European heatwave (a-e) and 2010 Moscow heatwave (f-j). Sub-figures show Hovmöller plots of the zonally averaged zonal wind (a, f), zonally averaged temperature anomalies (b, g) and meridional wave number $l^2$ (c, h). Here the black (white in h) lines mark the waveguides' turning points (solid for wave 7 and dashed for wave 6). QRA detection for k=5.5, 5.6, …, 8.4 is shown in Sub-plots (d, i). The relevant areas for resonance ($k = m \pm 0.2$ with $m = 6{,}7{,}8$) are shown in colors of higher saturation. The color scale illustrates the number of consecutive resonance days meeting the QRA conditions. Days/wave numbers fulfilling conditions i.) and ii.) but failing the AT are masked in grey. In e, j) amplitudes of the meridional NH-midlatitudinal wind field of wave 6, 7, 8 are shown in units of standard deviation with respect to the seasonal (JJA) climatological mean. Amplitudes exceeding a standard deviation of $\sigma = 1.5$ are shown in red.*

**Fig. 2:** *Distribution of duration of detected episodes for condition i, ii and after applying the AT for waves 6, 7 and 8. The bin width was set to 4. The majority of detected events are smaller than 8 days.*

**Fig. 3:** *Anomalies of probability density distributions of wave speed vs. wave amplitude during detected QRA events for waves 6 (left column), 7 (middle column), 8 (right column) after applying conditions i. (top row), i.+ii. (middle row) and i.+ii.+ AT (bottom row). Anomalies are shown in colored contours on top of JJA climatology* (black solid curves). *Positive anomalies (red) are observed in the area of slow moving high-amplitude waves for detected QRA-days, while the density of low amplitude fast waves is reduced (blue).*

**Fig. 4:** *Probability density distribution of amplitudes of quasi-stationary waves (*$c = \pm 2\ m/s$*) at 300 mb of days detected when applying conditions i., i.+ii and i.+ii.+ AT rows) of wave 6, 7, 8 (columns) during 1979 – 2014 summer (red) compared to days when respective conditions weren't met (black). Except for the pairing condition i./wave 8 (upper right) an overall shift in the distribution towards higher amplitudes is observed. Subplots marked with a red 'X' show statistically significant shifts (see Appendix, Table S1).*

**Fig.5:** *Hovmöller plots of zonally averaged zonal wind, phase speed as absolute values and respective wave amplitudes during the nine longest detected resonance episodes that coincide with observed wave amplitudes above 1.5σ of the climatology. Wave amplitudes are given in units of standard deviation from JJA climatology. Therefore no values are given for May and September (dark grey). The subfigures are aligned in time by the first resonance day (day "0", marked with a solid vertical black line), while giving a 35 days lead and lag period. The detected*

*QRA periods and their durations are marked with horizontal solid black lines at the bottom. Vertical dashed lines are marking the months. The majority of events are wave 7 events falling in the period after year 2000. QRA is often associated with a double jet pattern in the zonally averaged zonal wind.*

**Fig. 6:** *Probability density of lead lag times of a maximum amplitude within a window of* $\pm 14$ *days relative to the first day of QRA detection ('day 0'). Only long duration events coinciding with a wave amplitude of <1.5σ are included (25 events). A maximum (marked with a red dashed line) is observed at a time lag of about 6 days.*

**Fig. 7:** *15 day running mean meridional wind fields (line contours, South - North: blue, dashed, North - South: red, zero-line: black, long-dashed) and 15 day running mean temperature anomalies (color shading) of the NH mid-latitudes during the nine longest resonance episodes detected (as in Fig. 5 and Tab. A2). Wind velocities and temperature anomalies are averaged over the 15 days centered on the day with the highest wave amplitude within the respective QRA period. Landmass is depicted in dark grey by the respective coastlines.*

**Fig. 8**: *Probability density plots of MEX-index derived from daily temperature anomaly fields. Densities are shown for all QRA events of wave 6 – 8 (red dashed line) and QRA events of wave 6 – 8 of a minimum duration of 14 (red solid line) in comparison with Non – QRA days. The ensemble size is given in the lower left corner. Long QRA events show an increase in daily heat extremes, while there doesn't seem to be a relation between precipitation and QRA.*

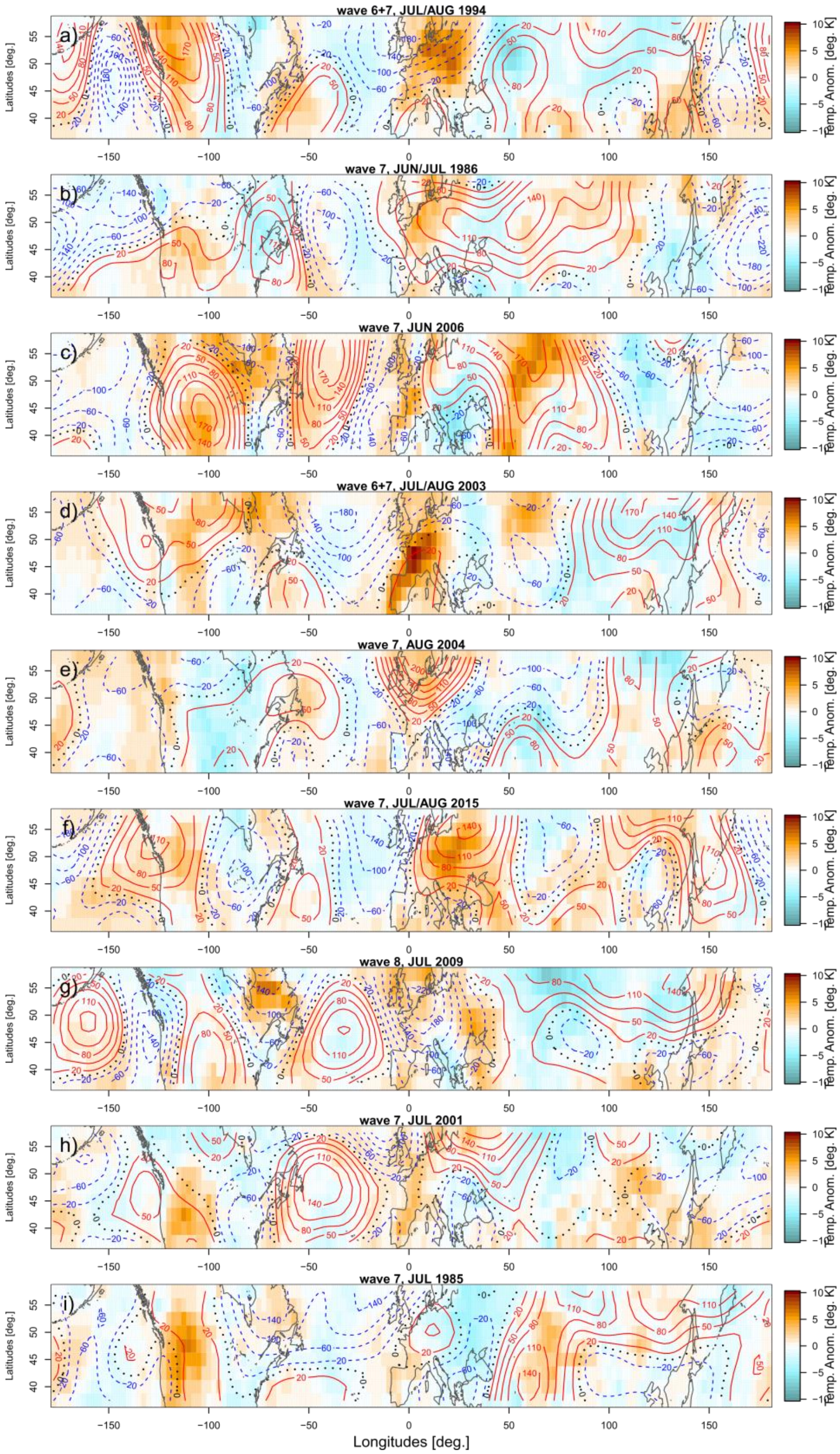


**Fig. A1:** *The 15 day running mean fields of the azonal geopotential height (line contours, South - North: blue, dashed, North - South: red, zero-line: black, long-dashed) and temperature anomalies (filled contours) of the NH mid-latitudes during the nine longest resonance episodes* *detected (as in Fig. 5, Fig. 7 and Tab.A2). Geopotential height - and temperature anomalies are averaged over the 15 days centered on the day with the highest wave amplitude within the respective QRA period. Landmass is depicted in dark grey by their coastlines.*

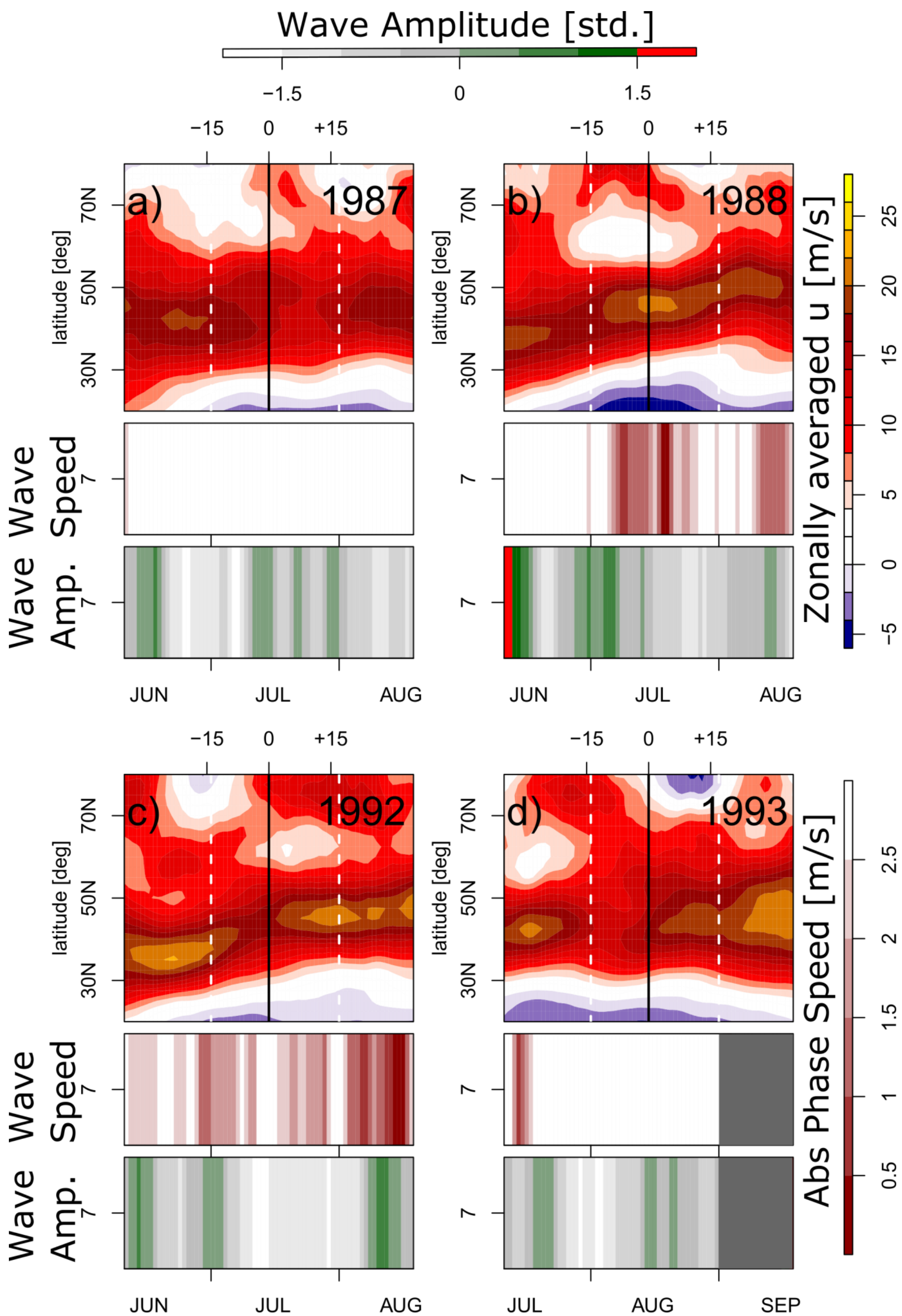

**Fig. A2:** *Data as in Fig. 5 showing exemplary summer days without QRA being detected.*

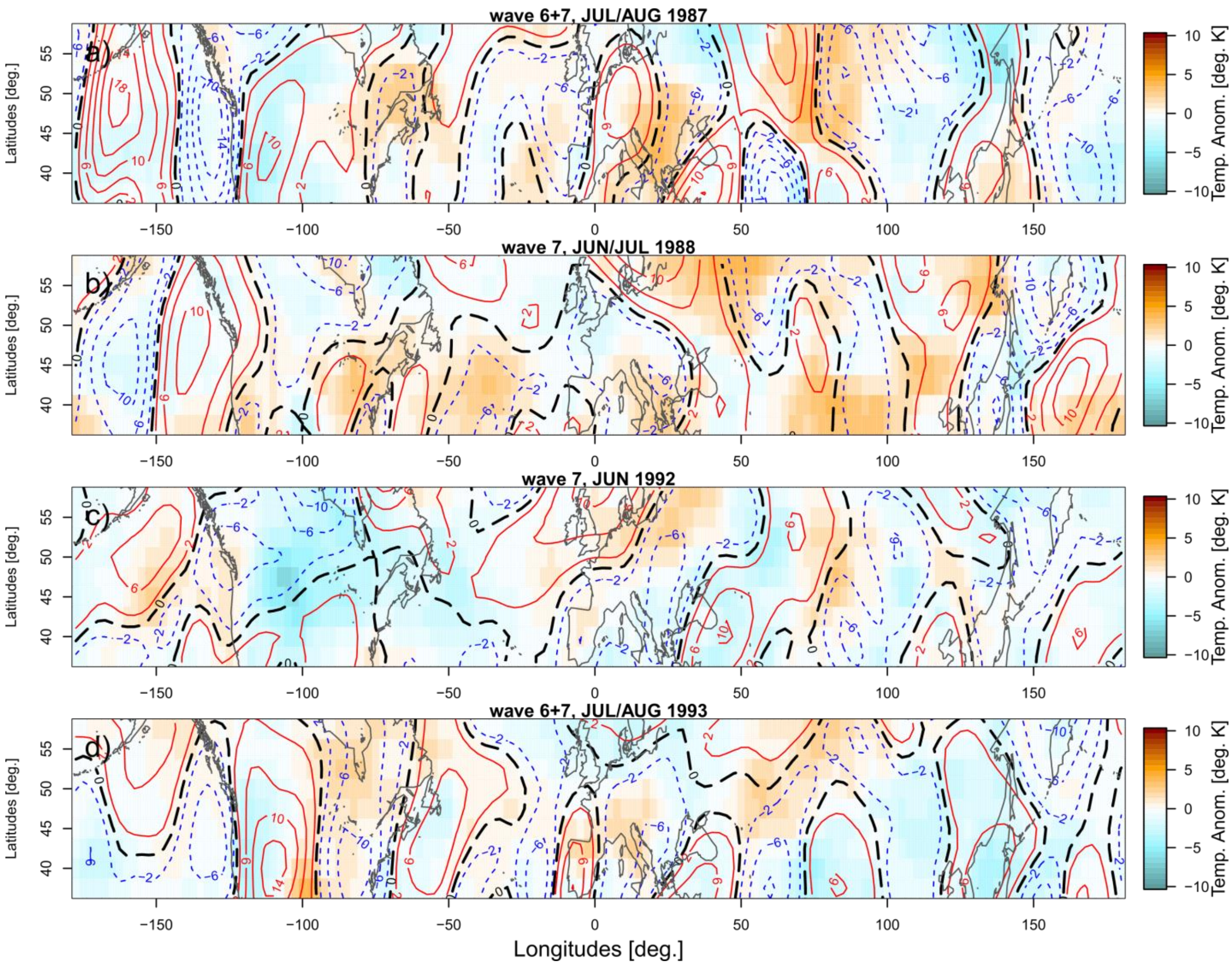


**Fig. A3:** *As in Fig. 7, temperature anomalies (shading) and v-winds (coloured line contours: red, Northward flow; blue, Southward flow), during those exemplary Non-QRA episodes depicted in Fig. A2.*